An IR-UWB Transmitter using Pulse Injection

Nontapat Channarong and **Kritsapon Leelavattananon**†, Non-members

ABSTRACT

This work presents a new pulse-shaping technique for an impulse-radio ultra-wideband (IR-UWB) transmitter which is intended for RFID tags and wireless sensor applications. The proposed pulse is derived from a rectangular pulse with its side-band energy suppressed in order to satisfy the FCC UWB regulation, in particular at low frequency band (3.1 - 4.8 GHz). To verify its effectiveness, the new pulse generator was designed in a 180-μm CMOS process. The simulation results indicate that the spectrum of the transmitted pulse can be fitted within the FCC UWB spectral mask. The total circuit consumes 926 μW at a 10 MHz pulse repetitive frequency (PRF).

Keywords: Impulse-radio ultra-wideband (IR-UWB), low-power, pulse generator, pulse shaping, transmitter.

1. INTRODUCTION

Impulse-radio ultra-wideband (IR-UWB) communication uses short pulses to transmit information. These pulses can propagate through radio channels without a need for a frequency conversion as commonly used in a narrow-band communication. This allows the implementation of the transmitter to be simple, and hence potentially consuming less power. This suits the implementation of RFID tags and wireless sensor applications, particularly with a battery-powered and/or an energy-harvesting feature. The short pulses are also more robust against multipath interferences. Additionally, they have a fine time-domain resolution suitable for positioning applications. The spectrum of the transmitted pulses is required to satisfy regulations such as the Federal Communication Commission (FCC). Many different pulse-shaping techniques have been proposed to shape the transmitted pulse to fit the FCC spectral mask, for operating both in the low frequency band (3.1 - 4.8 GHz) and the high frequency band (6.0 - 10.6 GHz). In the high frequency band, it is further from the existing commercial narrow band systems, which produces less interference to these radio systems. Hence, the regulation of spectrums around this band is less strict. This enables the use of simple pulse shaping techniques. Also, the receiver does not suffer from nearby strong interferences. High data rate communications can be achieved by using the IR-UWB in the high band [1–3]. However, high frequency devices are needed, which add extra costs. For the low frequency band, low and moderate data rate IR-UWB systems typically operate in this band. It is more suitable for low-power wireless communications. The FCC UWB regulation limit between 960 - 1610 MHz is tighter with –75.3 dBm/MHz. Hence, designing the pulse shaping is more difficult to satisfy the FCC UWB requirement. There have been various filtering approaches that were proposed to fulfil this requirement, such as raised-cosine pulse-shaping [4] and Gaussian pulse-shaping [5–7]. However, these pulse shapings must be accurate, which are quite difficult to achieve due to the very short duration of the transmitted pulse. Simple solutions in [8–15] proposed to inject a rectangular current pulse into a load or a filter as a way to filter out the unwanted spectral energies. This approach is simple to implement and achieve low energy consumption. However, increasing a pulse width (decreasing bandwidth) and using the filter with a large loaded quality factor to reduce the side-band energies, may still not be sufficient to fit the FCC UWB spectral mask, particularly at the low frequency band. The large loaded quality factor can also cause an insertion loss and filter out some of the wanted energy (in-band), leading to a reduction in the energy efficiency. An all-digital IR-UWB transmitter [16, 17] requests an off-chip filter. However, the details of the filter are not discussed. An entire UWB spectrum with in-band notch [18] provides the higher data rate, and the better resolution in the positioning applications.

In this work, a new pulse-shaping technique is presented. The proposed pulse is derived from a rectangular pulse, with additional pulse injection to suppress its spectral content around the 960 - 1610 MHz frequency band. This allows the transmitted pulse to satisfy the FCC UWB regulation, without requiring the use of any high order filter. Next, a spectrum analysis and a nonideal analysis are presented, which are based on the same theory. These analyses are useful to realize a pulse generator circuit and make the transmitted pulse to fulfil the FCC UWB spectral mask.

2. PULSE SHAPING

The proposed pulse shaping is constructed from a combination of two rectangular pulses: One will be

Manuscript received on June 8, 2019 ; revised on July 20, 2019 ; accepted on August 5, 2019.

The authors are with Department of Electronics, Faculty of Engineering, King Mongkut's Institute of Technology Ladkrabang, Bangkok, Thailand. E-mail : kritsapon.le@kmitl.ac.th

†Corresponding author.

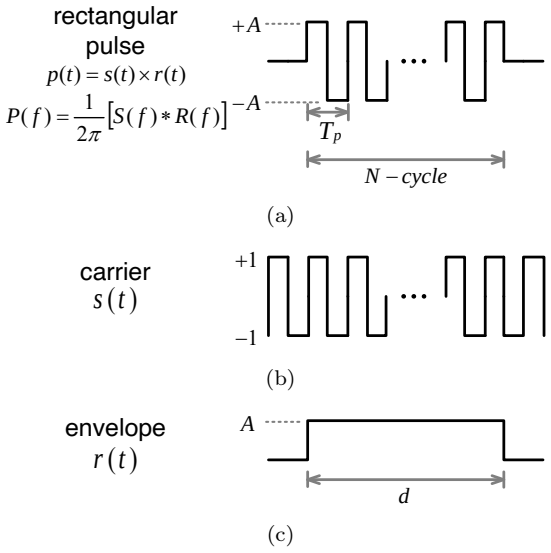

Fig.1: *Model of N cycles rectangular pulse, (a) rectangular pulse (b) square wave and (c) rectangular function.*

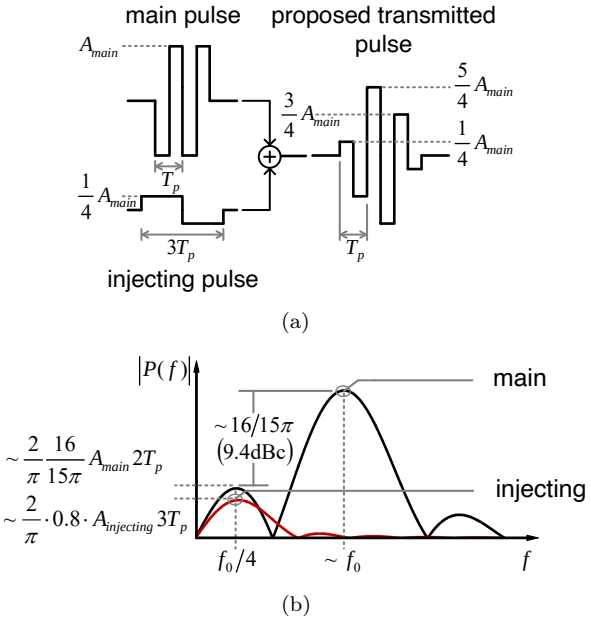

Fig.2: *(a) Proposed pulse shaping and (b) estimated spectrum of main pulse and injecting pulse.*

referred to as a main pulse. This pulse carries the information to be transmitted. The center frequency of the transmitted pulse is derived from this pulse. Another pulse, which is called an injecting pulse, is used to suppress the low frequency side-band energy of the main pulse that may violate the FCC UWB spectral mask.

2.1 Pulse Shape Analysis

An N cycles rectangular pulse [13], as shown in Fig. 1(a), can be represented by a multiplication of a square wave (carrier in Fig. 1(b)) with a period T_p (where $T_p = 1/f_0$) as in Eq. (1) and a rectangular function (envelope in Fig. 1(c)) with a width d (where $d = N \cdot T_p$) as in Eq. (2).

$$s(t) = \frac{4}{\pi}\sum_{n-1}^{\infty}\frac{1}{2n-1}\sin(2n-1)2\pi f_0 t \qquad (1)$$

$$r(t) = Au(t+\frac{d}{2}) - Au(t-\frac{d}{2}) \qquad (2)$$

where A is the height of the rectangular function, which determines the amplitude of the rectangular pulse. To simplify the spectrum analysis for finding a relationship between the main-lobe and the side-lobe, the harmonics of the square wave in Eq. (1) will be omitted. This is because the harmonic components, which arise due to the square wave, are far from the fundamental component. Hence, a side-band rejection, (where side-band rejection is the ratio of the energy spectral density at a specified side-band (P_{side}) to the energy spectral density at the center frequency (P_{center})), is slightly affected from the harmonics. Also, the high-order harmonics are suppressed by the limited bandwidth of the circuit. Thus, the frequency domain of the square wave at the fundamental frequency can be expressed as

$$S(f) = j4\Big[\delta(\pi(f+f_0)) - \delta(\pi(f-f_0))\Big] \qquad (3)$$

The frequency domain of the rectangular function in Eq. (2) is given by

$$R(f) = Ad\,\mathrm{sinc}(\pi f d) \qquad (4)$$

Thus, the frequency domain of the rectangular pulse can be expressed as

$$P(f) = -j\frac{2}{\pi}Ad\Big[\,\mathrm{sinc}(\pi(f-f_0)d) - \mathrm{sinc}(\pi(f+f_0)d)\Big] \qquad (5)$$

The –10-dB bandwidth is determined by the sinc function which can be approximated as

$$BW_{-10dB} = \frac{4.6}{\pi d} = \frac{4.6}{\pi}\cdot\frac{f_0}{N} \qquad (6)$$

For the proposed pulse shaping, a 2-cycle rectangular pulse with a period of T_p is used as the main pulse, as shown in Fig. 2(a). Since the low frequency side-band of this pulse has only one lobe, it is possible to suppress this lobe by injecting another signal which can negate with this lobe. Its spectrum can be calculated using Eq. (5), and is shown in Fig. 2(b). The center frequency of the spectrum is approximately $1/T_p$ (f_0). The low frequency side-lobe peaks at around $f_0/4$. To simplify the analysis, the center frequency and the peak of the side-lobe will be approximated to be at f_0 and $f_0/4$, respectively. The side-band rejection is approximately

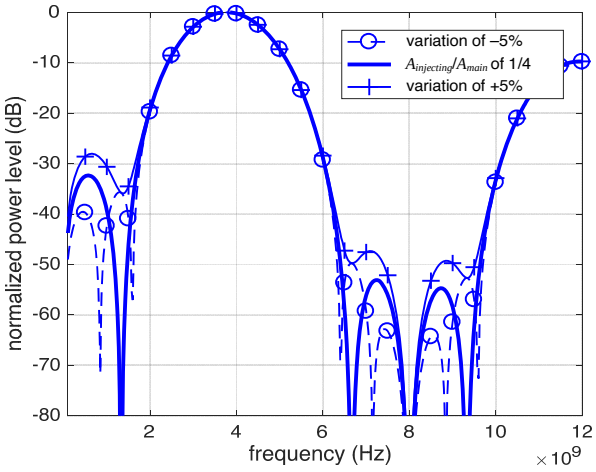

Fig.3: *Spectrum of proposed pulse with varied injecting pulse amplitude to main pulse amplitude ratio.*

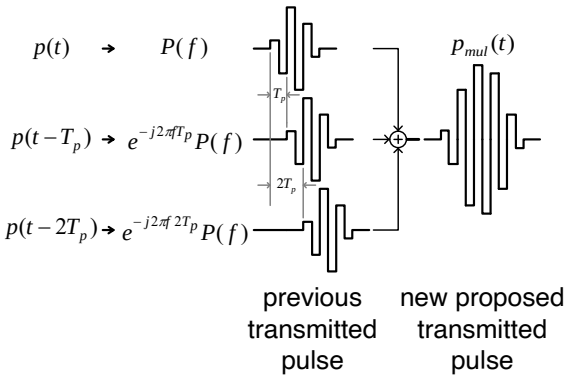

Fig.4: *Proposed transmitted pulse with multiple pulses.*

16/15π (–9.4 dBc). For the IR-UWB systems that operate in the low frequency band, the spectral content of the side-lobe that locates around $f_0/4$ is the part in violation of the 960 - 1610 MHz band of the FCC UWB regulation. It requires the side-band rejection to be more than –35 dBc. The energy of the low frequency lobe of the main pulse therefore needs further suppression. This can be achieved by injecting a signal which has the same spectrum as the low frequency side-lobe of the main pulse, but is opposite in phase. The injecting pulse is therefore chosen to be a 1-cycle rectangular pulse with a period of 3 times of the main pulse ($3T_p$) and opposite phase with respect to the main pulse. Its center frequency is located at around $f_0/4$ (at the peak of the low frequency side-lobe of the main pulse). The amplitude of the injecting pulse, $A_{injecting}$, is related to the amplitude of the main pulse, A_{main}. The spectrum of the main pulse and the injecting pulse can be calculated by using the relationship in Eq. (5). At the peak of the low frequency side-lobe of the main pulse (at the $f_0/4$), the amplitude of the spectrum of the main pulse can be written as

$$P_{main}(f)\Big|_{f=f_0/4} = -j\frac{2}{\pi}\frac{16}{15\pi}\cdot A_{main}2T_p \qquad (7)$$

and the amplitude of the injecting pulse can be written as

$$P_{injecting}(f)\Big|_{f=f_0/4} = -j\frac{2}{\pi}\cdot 0.8\cdot A_{injecting}3T_p \quad (8)$$

where T_p is the period of the main pulse (carrier period). If the peaked amplitude of the spectrum of the main pulse and the injecting pulse is assigned to be equal, the relation between the amplitude of the main pulse and the amplitude of the injecting pulse can be expressed as

$$A_{injecting} = \frac{8}{9\pi}\cdot A_{main} \qquad (9)$$

The spectrum of the injecting pulse will not be perfectly matched with the shape of the spectrum of the low frequency side-lobe of the main pulse. To get an insight into a reasonable ratio of the injecting pulse amplitude to the main pulse amplitude, a quantitative analysis of the proposed transmitted pulse is used. The function of the proposed transmitted pulse, which is the combining of the main pulse function (2-cycle rectangular pulse with a period of T_p) and the injecting pulse function (1-cycle rectangular pulse with a period of $3T_p$), can be obtained by applying Eq. (5). In our design, the injecting pulse amplitude is chosen to be a quarter of the main pulse amplitude, $A_{injecting} = A_{main}/4$, as shown in Fig. 2(a). Its spectrum is shown in Fig. 2(b). The spectrum of the proposed transmitted pulse depends on the ratio between $A_{injecting}$ and A_{main}. Fig. 3 shows the spectrum of the proposed transmitted pulse when the ratio $A_{injecting}/A_{main}$ varies within $\pm 5\%$ of the nominal ratio (1/4). The low frequency side-band rejection is sensitive to the ratio of the injecting pulse and the main pulse. Since the low frequency side-lobe energy is required to be very low, the ratio of the two pulses needs to be controlled to be fairly accurate.

With the proposed transmitted pulse derived from a 2-cycle main pulse, its bandwidth will be large. To transmit a narrower bandwidth pulse, the width of the transmitted pulse needs to be widened. This can be achieved by combining many of the proposed transmitted pulses together, where each of the proposed transmitted pulses overlaps each other. Each of the adjacent pulses is shifted by one period of the carrier period (T_p), as shown in Fig. 4. Each of the previous transmitted pulses which is shifted by an integer number of the carrier period (nT_p) is related to the phase shift of the frequency spectrum as the time shifting property of the Fourier transform. Thus, the frequency domain of the new proposed transmitted pulse with the multiple pulses can be expressed as

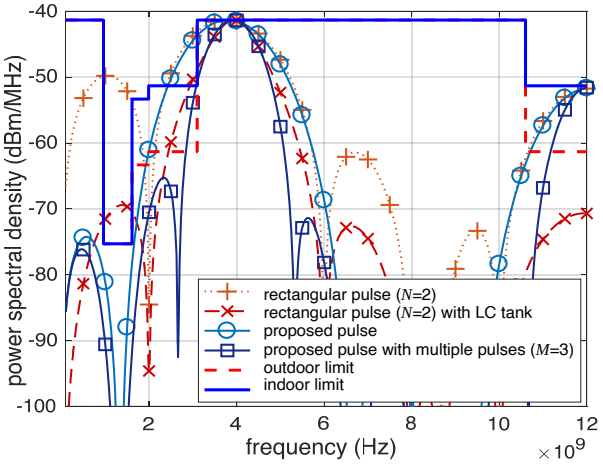

Fig.5: *Simulated spectrum of different pulse shapings.*

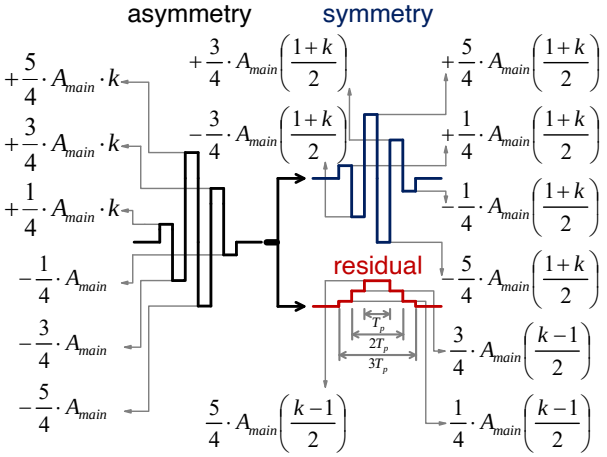

Fig.6: *Asymmetric waveform model with amplitude mismatch.*

$$P_{mul}(f) = \Big[1 + e^{-j2\pi fT_p} + e^{-j2\pi f2T_p} + \cdots + e^{-j2\pi f(M-1)T_p}\Big] P(f) \quad (10)$$

where $P(f)$ is the frequency domain of the previous proposed transmitted pulse and M is the number of previous transmitted pulses. The phase of the first previous transmitted pulse and its shifted version are a linear function of the frequency and become the same at the center frequency (and harmonics). The spectrum of these pulses will add to each other at the center frequency. Hence, the combined multiple pulse exhibits narrower bandwidth, while its side-band rejection is maintained to be more than –35 dBc in the 960 - 1610 MHz band. The side-band rejection can be calculated by using the quantitative analysis in Eq. (10). For the new proposed transmitted pulse with the multiple pulses ($M = 3$) with a carrier period of 250 ps (f_0 =4 GHz), its side-band rejection is improved by 8.5 dB at a side-band frequency of 960 MHz.

For the repetitive pulse train, the spectrum of the repetitive pulse train exhibits strong spectral lines (spikes) at multiples of the pulse repetition frequency (PRF). The energy spikes of the transmitted pulse will be spread by using a data modulation and a randomizing pulse train. The power spectral density of the repetitive pulse train can be calculated from the Fourier transform function by using the relationship between Fourier transform and Fourier series, as $C_n = X(n\omega_0)/T$, where C_n is the exponential Fourier series coefficients, $X(\omega)$ is the Fourier transform of a pulse and T is a period of the pulse trains, $\omega_0 = 2\pi/T$. The power spectral density (PSD) of the proposed transmitted pulse at the center frequency can be estimated by applying Eq. (5). The 3rd harmonic component of the injecting pulse must be considered since it locates at around the center frequency of the main pulse. It has a magnitude of 1/3 of the main pulse at its center frequency. Suppose the load is a 1-Ω resistive load, the PSD at the center frequency can therefore be expressed as

$$P = \frac{1}{2}\left(\frac{2}{T}\left[\underbrace{\left(\frac{2}{\pi}\cdot A_{main}\cdot 2T_p\right)}_{\text{main}} + \underbrace{\left(\frac{2}{3\pi}\cdot 0.8\cdot\frac{A_{main}}{4}\cdot 3T_p\right)}_{\text{3rd harmonic of injecting}}\right]\right)^2 \quad (11)$$

The PSD of the multiple pulses at the center frequency is multiplied by a factor of M squared where M is the number of pulses. Power evaluations of a modulated pulse train was described in [5].

Fig. 5 shows the spectrum of different pulse shapings where their center frequencies are at 4 GHz (T_p =250 pS), and compared to the FCC spectral mask. The unwanted side-band of the rectangular pulse ($N = 2$) can be further suppressed by 20 dB using an LC tank with a loaded quality factor of 3. However, this suppression is not enough for the rectangular pulse where its center frequency locates close to the low frequency edge of the spectral mask. For the proposed transmitted pulse, the spectrum of a single pulse occupies over the whole FCC UWB spectral mask. The spectrum of the new proposed transmitted pulse with multiple pulses has narrower bandwidth and lower side-band energy, which therefore satisfies the FCC spectral mask.

2.2 Nonideal Pulse Shape

The nonideal waveforms cause an unwanted spectral energy, which may violate the FCC spectral mask. As shown in Fig. 6, an asymmetric waveform

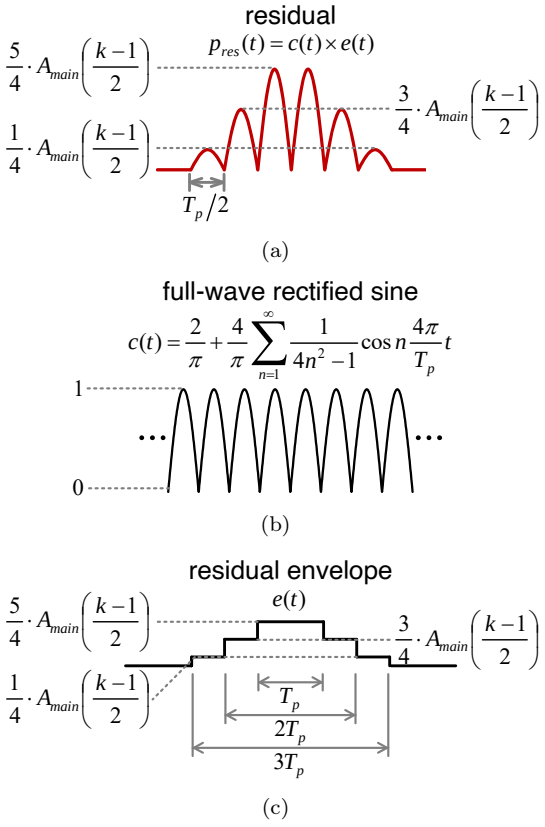

Fig. 7: *Asymmetric waveform model with nonzero transition time; (a) residual, (b) full-wave rectified sine and (c) residual envelope.*

model with an amplitude mismatch $(1-k)\cdot 100\%$ between a positive amplitude and a negative amplitude can be separated into two parts. These are: a symmetric pulse (ideal) and a residual part. The residual can be represented by the combination of a rectangular function with a height of $0.125A_{main}(k-1)$ and a width of $3Tp$, a rectangular function with a height of $0.25A_{main}(k-1)$ and a width of $2Tp$, and a rectangular function with a height of $0.25A_{main}(k-1)$ and a width of Tp. Hence, the frequency domain of the residual can be expressed as

$$P_{res,zero}(f) = A_{main} \cdot \frac{k-1}{2} \cdot T_p \cdot \left\{ \frac{3}{4} \operatorname{sinc}(\pi f \cdot 3T_p) + \operatorname{sinc}(\pi f \cdot 2T_p) + \frac{1}{2} \operatorname{sinc}(\pi f \cdot T_p) \right\} \quad (12)$$

The spectrum of the residual is the combination of the sinc functions and its frequency is centered at the zero frequency. Hence, its spectrum appears at the low frequency side-band of the symmetric pulse spectrum. The contribution of the residual spectrum can cause a violation in the 960 - 1610 MHz band. For the nonideal pulse shape model of the new proposed transmitted pulse with multiple pulses ($M = 3$), the acceptable amplitude mismatch is about $\pm 9\%$. In

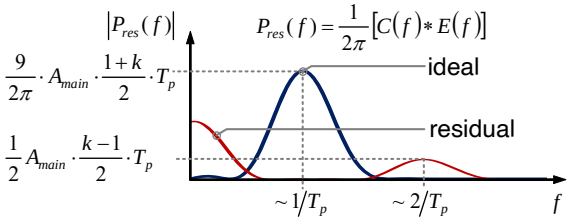

Fig. 8: *Spectrum of asymmetric waveform model with nonzero transition time.*

practice, an ideal square wave with a zero transition time is impossible because their harmonics are suppressed by the limited bandwidth of the circuit. The proposed transmitted pulse exhibits smoother transitions. To simplify the analysis of this case, a sinusoid modulated pulse (proposed transmitted pulse) is employed to represent a nonzero transition time model of the proposed transmitted pulse. The proposed transmitted pulse is multiplied by a full-wave rectified sine with a period of $T_p/2$ (half of the proposed pulse's carrier period). The harmonics of the proposed transmitted pulse are eliminated, which reduce the complexity of the analysis. Hence, the asymmetric waveform in this case can be modeled as a multiplication of the asymmetric waveform, with a zero transition time (Fig. 6), and the full-wave rectified sine as well. Therefore, the residual becomes the waveform as seen in Fig. 7(a), which can be represented as a multiplication of the full-wave rectified sine (Fig. 7(b)) and the residual envelope (Fig. 7(c)). The residual envelope is the same function as in Eq. (10). Because the harmonic components of the full-wave rectified sine are always outside of the UWB band, they can be neglected. Thus, the frequency domain of the residual can be expressed as

$$P_{res}(f) = \frac{1}{2\pi} \Bigg\{ \underbrace{\left(4\delta(f) - \frac{4}{3}\left[\delta(\pi(f+2f_0)) + \delta(\pi(f-2f_0))\right]\right)}_{\text{full-wave rectified sine}} * E(f) \Bigg\} \quad (13)$$

where $f_0 = 1/T_p$ and $E(f)$ is the frequency domain of the residual envelope function in Eq. (12). The first term in the frequency domain of the full-wave rectified sine is the zero frequency component while the second term is the fundamental component that is centered at $2f_0$. This means that the spectrum of the residual envelope will be converted to around the fundamental frequency of the full-wave rectified sine. The zero frequency lobe of the residual is a multiplication of the residual envelope in Eq. (12) and a factor $4/2\pi$ (–3.9 dB). In other words, the zero frequency lobe of the residual of the nonzero transition time model is suppressed by 3.9 dB relative to the zero

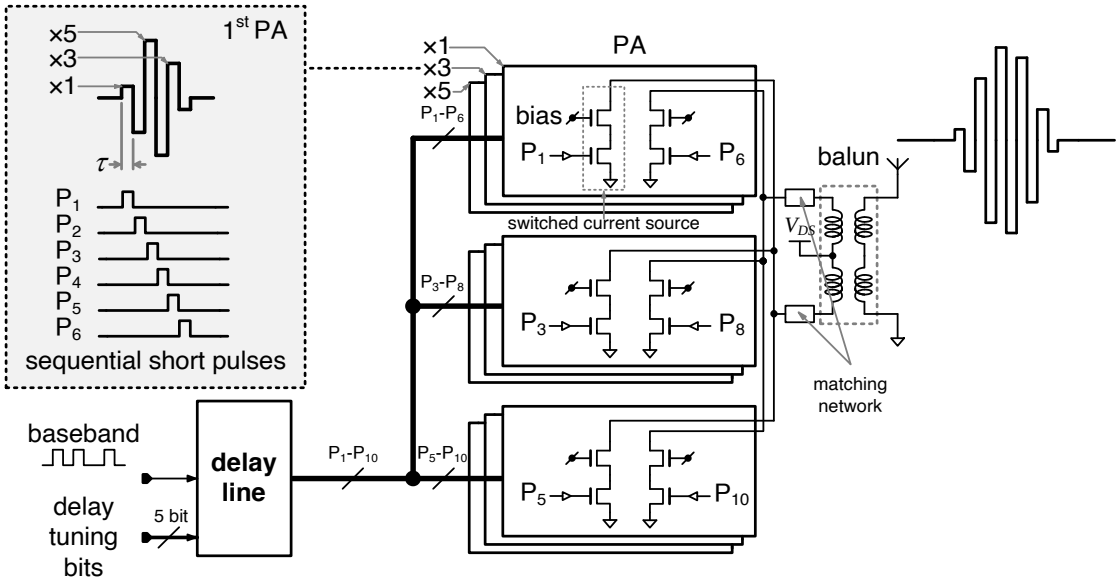

Fig.9: *Circuit diagram of proposed pulse generator.*

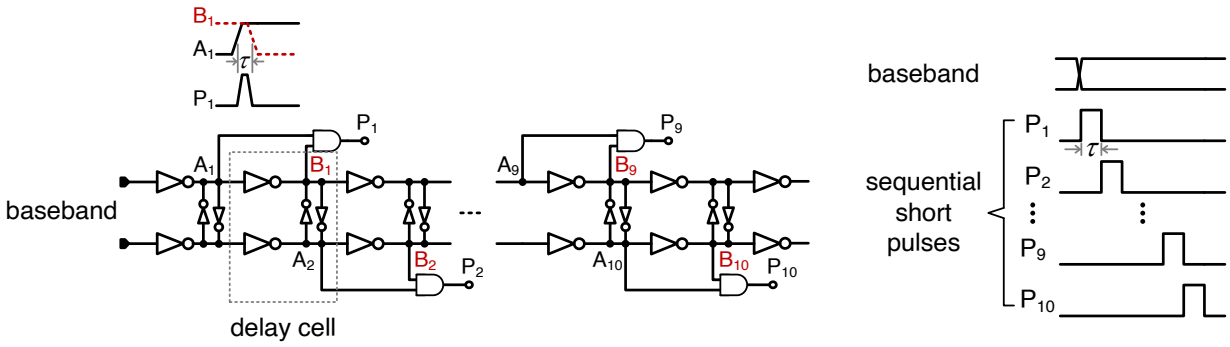

Fig.10: *Circuit diagram of the delay line. Each of stages is composed of delay cells connected with AND gate.*

transition time model. The spectrum of this residual is shown in Fig. 8. Although its fundamental lobe is possibly within the UWB band when operating in the low frequency band, it can be neglected because its energy is low relative to the energy of the symmetrical wave. This may only interfere within the UWB band itself. The zero frequency lobe of the residual is dominant because the constraint at 960 MHz is very strict. For the new proposed transmitted pulse with multiple pulses ($M = 3$), the acceptable amplitude mismatch become $\pm 15\%$. The zero transition time model is therefore the worst case. The essential causes of the inaccuracy in the pulse's shape that are related to the actual circuit implementation will be described in Section 3.2.

3. CIRCUIT IMPLEMENTATION

3.1 IR-UWB Pulse Generator

In this work, the proposed transmitted pulse with multiple pulses ($M = 3$) is used to demonstrate the concept of the proposed pulse shaping. The proposed pulse generator is shown in Fig. 9. It consists of three push-pull power amplifiers (PAs) in parallel and a delay line. Replica circuits (the PAs and the delay line) reduce the complexity of the circuit implementation. The bias at the drain of the PAs is supplied through a center tap of a balun. Three proposed pulses that overlap each other with a time shift of T_p are generated by the three PAs. Each of the PAs acts as a piecewise current source to shape the proposed pulse (in Fig. 2(a)). It is composed of six switched current sources with a multiplication factor of 1/4, 3/4, 5/4, 5/4, 3/4, and 1/4 times of the main rectangular pulse amplitude. In the least multiplication factor switched current sources, the size of current source transistors and switch transistors is $W/L = 4.00\mu m/0.18\mu m$. These six switches are controlled, respectively, by sequential short pulses P_1, P_2, P_3, P_4, P_5, and P_6 for the first PA, and $P_3 - P_8$ and $P_5 - P_{10}$ for the second PA and the last PA, respectively. The magnitude of

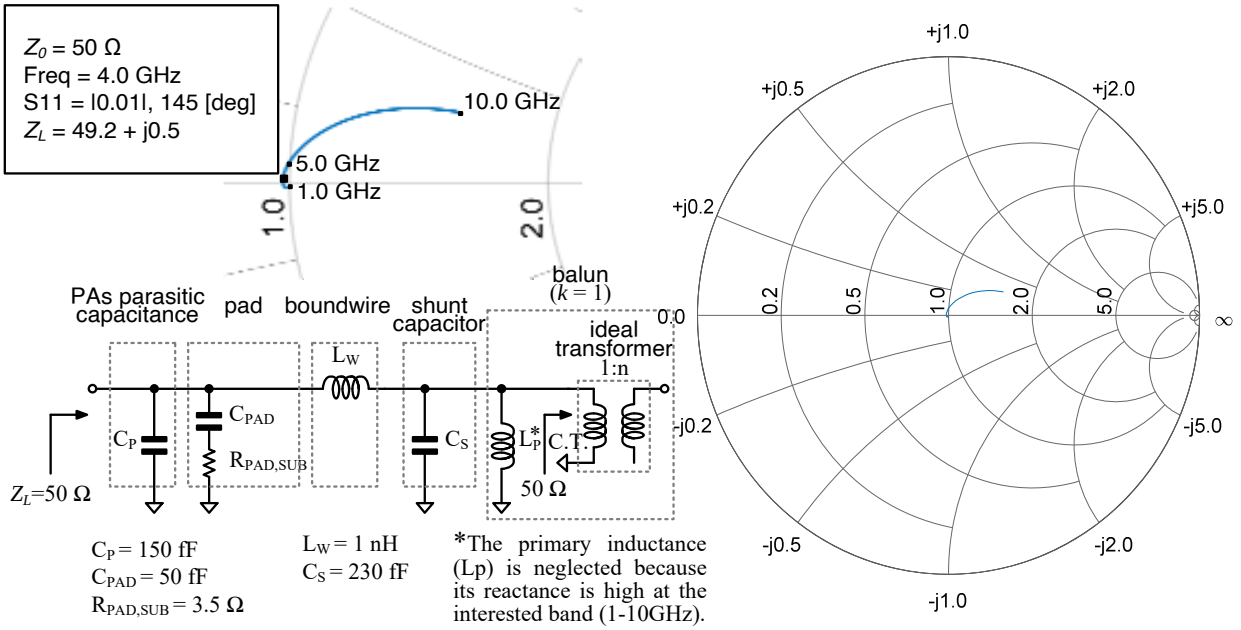

Fig.11: *Output matching network and load impedance.*

the proposed transmitted pulse, which relates to the main pulse amplitude, determines the energy of the transmitted pulse. It can be varied by changing the current source's bias. For the transmitted pulse with a PRF of 10 MHz and a 50-Ω load, the main pulse amplitude is chosen to be 2.4 mA in order to emit peak power around –42.0 dBm/MHz. The sequential short pulses with a pulse width of $T_p/2$ are generated from the delay line, as shown in Fig. 10. Each of these pulses is obtained by propagating the input signal (baseband) through a delay cell (inverter). The input signal and the propagated signal (output signal of delay cell) are then passed through an AND gate. The pulse width of the sequential short pulses is determined by the propagation delay of the delay cell, τ. The center frequency of the transmitted pulse is inversely proportional to the pulse width of the sequential short pulses. It can be digitally tuned by a variable capacitive load which is a 5 bit binary-weighted capacitor bank. The center frequency has a nonlinear behaviour with the binary code. However, the purpose of the variable center frequency is to only keep the spectrum to be placed within the spectral mask over the PVT variation. This digitally controlled delay line (DCDL) structure has a potential to operate like a delay-locked loop, which can be utilized to calibrate the delay cells that is independent from the PVT variation. However, the DCDL with fine resolution requires the use a large transconductance, leading to a high power consumption. In this work, the pulse width of the sequential short pulses were tuned to be around 125 ps for the center frequency at around 4 GHz. The sequential short pulses are square in shape, which also causes more harmonics in the transmitted pulse. These harmonics will need to be attenuated by limiting the bandwidth of the circuit.

3.2 Practical Considerations

The misshapen transmitted pulse as a result of the real circuit implementation can cause its spectrum to violate the spectrum mask. The nonideal effects, other than those previously mentioned in Section 2.2, are considered as follow:

1) The bandwidth of the pulse generator is limited by the parasitic capacitances, which are dominant at the outputs of the PAs. Hence, the spectrum of the transmitted pulse is limited as well. The bandwidth of the pulse generator must be wide enough to cover the whole operation frequency in order to avoid any attenuation of the in-band energy, which will degrade the side-band rejection. These parasitic capacitances can be tuned out by a matching network.

2) The overlapping of the sequential short pulses will make the transmitted pulse misshapen. The total energy of the pulses that overlap each other is reduced. The reduction of the in-band energy is more than the reduction of low frequency side-band energy. Hence, the side-band rejection of the transmitted pulse is reduced. In order to avoid the overlapping of the sequential short pulses, a delay can be added to a signal path A_n of each delay cells to obtain narrower width for each sequential short pulses. The third order harmonic of the transmitted pulse can also be attenuated by controlling the width of the sequential short pulses. The bandwidth of the switched current sources and their drivers must be sufficiently wide. In practice, the high precision of a very short pulse

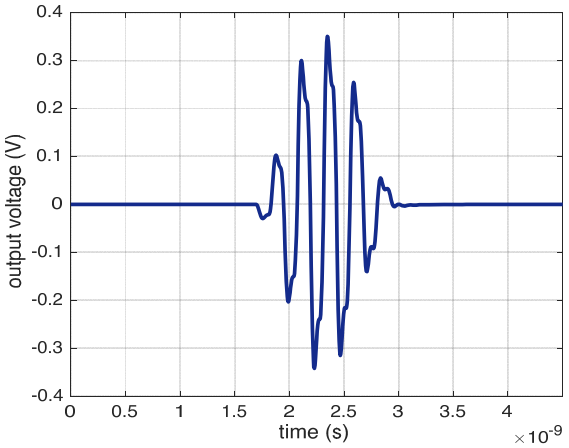

(a)

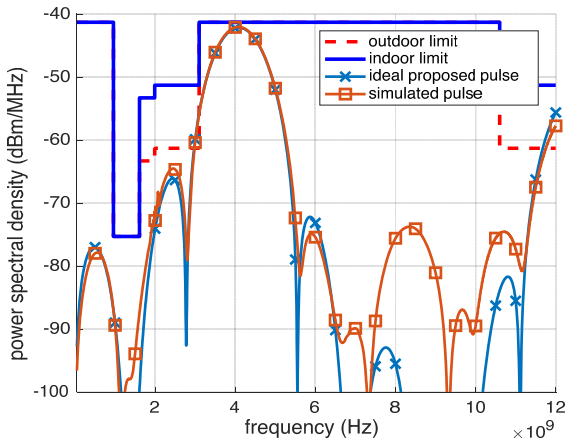

(b)

Fig.12: *(a) Simulated output waveform and (b) simulated power spectral density.*

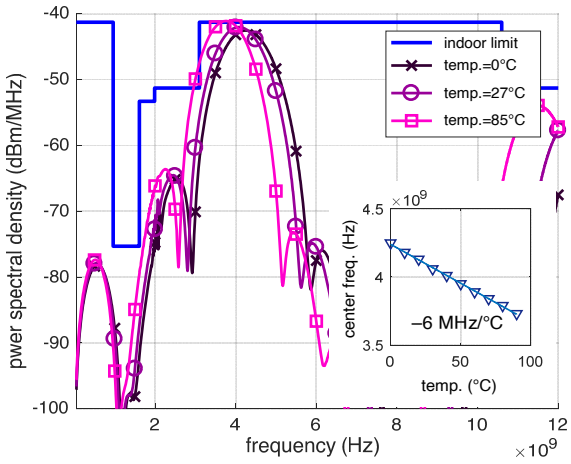

Fig.13: *Simulated power spectral density with temperature variations from 0° C to 85° C.*

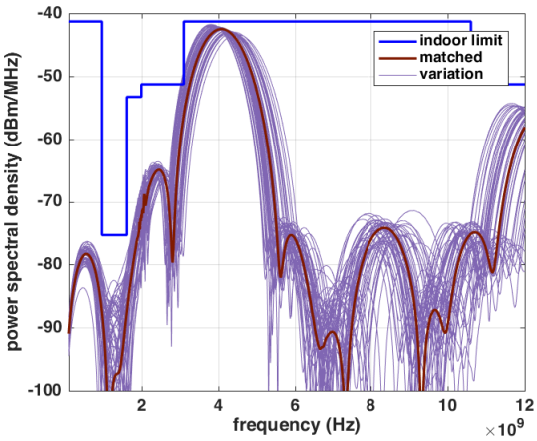

Fig.14: *Simulated power spectral density with Monte Carlo.*

is difficult to achieve. However, it will be improved with a smaller process technology.

In the practical implementation, these effects are acceptable, and usually reduced by the matching network. Fig. 11 shows an example of the output matching network and the load impedance. The matching network consists of a parasitic capacitance of the PAs, a pad capacitance, a bond wire inductance and a load capacitor (or an open-circuit stub). The load capacitor is added to tune the load impedance to 50-Ω. The operating frequency range of the output network is expanded over the specified frequency range (1 - 5 GHz) if the parasitic capacitance of the PAs, the pad capacitance, and the bond wire inductance are kept small enough. Although the bond wire inductance has a poor precision, it does not affect the violation of the spectral mask in the 960 - 1610 MHz band, which is a major concern. The accuracy simulation of the bond wire can be obtained by using an electromagnetic (EM) simulation [12]. The ideal transformer balun with a coupling coefficient k of 1 and a large primary inductance L_p is used in our simulations in order to avoid the limited frequency response of the circuit under test, which hides a realistic spectrum of the proposed transmitted pulse. The transformer model was described in [19]. The lower and upper cut-off frequencies are inversely proportional to $k^2 L_p$ and $(1-k^2)L_p$, respectively. The balun can be realized by an integrated monolithic transformer [19] and a microstrip Marchand balun [20].

4. SIMULATION RESULTS

The demonstrated pulse generator was implemented in a 0.18-μm CMOS process with a 1.8 V power supply. The load (antenna) of the pulse generator is assumed to be a 50-Ω resistive load. The transformer balun is modeled to operate over a wide operating frequency range.

Fig. 12(a) and (b) show the post-layout simulation results of the pulse generator output waveform and its PSD. Its spectrum is centered at around 4 GHz, and with a power of –42.0 dBm/MHz. The –10-dB bandwidth is at about 1.7 GHz. The sharp edge (rising/falling edges) of the simulated pulse results in

Table 1: *Comparison with other pulse generators.*

	[5]	[21]	[22]	[4]	[6]	[7]	This work
Process	0.18 μm[1]	0.18 μm	0.18 μm	0.18 μm	0.13 μm	28 nm	0.18 μm
Center freq. (GHz)	3.1-10.6[2]	4	4.5-4.8[3]	4	3.0-5.0	3.5-4.5	4
–10-dB BW (GHz)	426-558 MHz	2	3.5-6.5	1.4	1.8-3.5	1	1.7
Output swing (Vpp)	0.25 @ 4 GHz	0.195	1	1.28	0.9	0.35	0.7
Allowable maximum peak PSD (dBm)	–41.3	–41.3	<–50.0	–41.3	–41.3	–50.0	–41.3
Energy consumption (pJ/pulse)	373	190	86	825	147	24.3	92.6

[1]SiGe BiCMOS process
[2]Centered in 528-MHz-wide channels equally spaced within the ultra-wideband band.
[3]Variation range of the center frequency

stronger odd harmonics. The spectrum of the simulated pulse exhibits unwanted spectral components due to the inaccuracy of the pulse's shape. The mismatch between the positive amplitude and the negative amplitude introduces two extra lobes, one at the zero frequency and another at about 8 GHz (second order harmonic). Although the zero frequency is our main concern, it is attenuated by the primary inductance of the balun used in the simulation. As can be seen from Fig. 12(b), only the second order harmonic shows up in the spectrum of the simulated pulse. In reality, both the harmonics and the low frequency side-band can be greatly attenuated without using any additional high order filter.

Fig. 13 shows the simulated PSD with temperature variation from 0°C to 85°C. The center frequency of the transmitted pulse was designed to be at 4 GHz, at room temperature (27°C). The simulation result shows the designed pulse's spectrum to have the temperature coefficient of –6 MHz/°C. As can be seen, at high temperature the spectrum may violate the FCC spectral mask at the corner of the low frequency band (at 3.1 GHz). As the temperature deceases, the spectrum is shifted up. The low frequency side-band will be attenuated more by the primary inductance of the balun. The shifted center frequency of the transmitted pulse can be tuned back to the wanted frequency with the DCDL. This allows the spectrum of the transmitted pulse to fulfill the FCC requirement.

Fig. 14 shows the simulated result with Monte Carlo simulation (50 samples with 3σ process variations and local mismatch). As can be seen, the violation of some simulated spectrums occurs at the corner of the low frequency band because of the effect of the process variations in the DCDL, which causes center frequency variations. However, these spectrums can still be fitted within the FCC spectral mask when the center frequency is tuned back. The margin in the 960 - 1610 MHz band can be significantly increased just by using only a simple filter, or by employing the band pass property of the passive elements such as the balun and the antenna.

The power consumption of the pulse generator is 926 μW at a 10 MHz RPF or with an energy consumption per pulse of 92.6 pJ/pulse, about 74% of the total power is consumed by the delay line. This is mainly due to the fine resolution digital delay line.

Table 1 compares the results of this work with previously published works. The pulse generator in [5] was based on an up-converted Gaussian pulse. However, a high pass filter was required. A Gaussian pulse with a filter was employed in [21, 22]. These simpler approaches achieved better power performance. The pulse generator in [4, 6, 7] were based on a piecewise current source similar to this work. Accurate shapes of the raised-cosine pulse [4] and the Gaussian pulse [6] allow their spectrums to be fitted with FCC spectral mask. In [7], the advanced process allows for complexity of the circuit design with lower power consumption. The transmitted pulse, which used the Gaussian shape, cannot satisfy the spectral mask in the 960 - 1610 MHz band, although the theoretical analysis is able to fit the spectral mask.

5. CONCLUSION

The new pulse-shaping technique for the IR-UWB systems in the low frequency band has been proposed. The proposed pulse shaping is constructed by combining a rectangular pulse with an injecting pulse to suppress its side-band energy in order to meet the FCC UWB requirement. The demonstrated pulse generator was implemented in a 0.18-μm CMOS process. The post-layout simulation results show that the spectrum can be fitted within the FCC UWB spectral mask. The practical inaccuracies in the implementation of the pulse shaping mainly reduce the margin of the side-band rejection, in the 960 - 1610 MHz band. However, these inaccuracies are acceptable. The harmonic components are contributed by the switched current. The unwanted spectral components can be further suppressed by using a simple band pass filter. The band pass property also reduces the variations in spectrum. In practice, the additional filter is unnecessary because of the limited operation frequency of the passive elements in the circuit such as a balun and an antenna. The pulse generator is operated at 1.8 V supply voltage, and the power consumption is 926 μW at a 10 MHz PRF.

ACKNOWLEDGEMENT

The authors would to thank IC Design Section, Thai Microelectronics Center (TMEC), for supporting the chip fabrication.

References

[1] V. V. Kulkarni, M. Muqsith, K. Niitsu, H. Ishikuro, and T. Kuroda, "A 750 Mb/s, 12pJ/b, 6–to-10GHz CMOS IR-UWB Transmitter with Embedded On-Chip Antenna," *IEEE Journal of Solid-State Circuits*, vol. 44, no. 2, pp. 394-403, Feb. 2009.

[2] Y. Ying, X. Bai, and F. Lin, "A 1-Gb/s 6-10-GHz, Filterless, Pulsed UWB Transmitter With Symmetrical Waveform Analysis and Generation," *IEEE Transactions on Very Large Scale Integration (VLSI) Systems*, vol. 26, no. 6, Jun. 2018.

[3] R. Liu, B. R. Carlton, S. Pellerano, F. Sheikh, D. S. Vemparala, A. Ali, and V. S. Somayazulu,, "A 264-μW 802.15.4a-Compliant IR-UWB Transmitter in 22nm FinFET for Wireless Sensor Network Application," in *Proceeding of 2018 IEEE Radio Frequency Integrated Circuits Symposium*, pp. 164-167, Jun. 2018.

[4] T. Norimatsu, R. Fujiwara, M. Kokubo, M. Miyazaki, A. Maeki, Y. Ogata, S. Kobayashi, N. Koshizuka, and K. Sakamura, "A UWB-IR transmitter with digitally controlled pulse generator," *IEEE Journal of Solid-State Circuits*, vol. 42, no. 6, pp.1300-1309, Jun. 2007.

[5] D. D. Wentzloff, and A. P. Chandrakasan, "Gaussian Pulse Generators for Subbanded Ultra-Wideband Transmitters," *IEEE Transactions on Microwave Theory and Techniques*, vol. 54, no. 4, pp. 1647-1655, Apr. 2006.

[6] R. Vauche, E. Muhr, O. Fourquin, S. Bourdel, J. Gaubert, N. Dehaese, S. Meillere, H. Barthelemy, and L. Ouvry, "A 100 MHz PRF IR-UWB CMOS Transceiver With Pulse Shaping Capabilities and Peak Voltage Detector," *IEEE Transactions on Circuits and Systems I: Regular Papers*, vol. 64, no. 6, pp. 1612-1625, Jun. 2017.

[7] G. de Streel, F. Stas, T. Gurné, F. Durant, C. Frenkel, A. Cathelin, and D. Bol, "SleepTalker: A ULV 802.15.4a IR-UWB Transmitter SoC in 28-nm FDSOI Achieving 14 pJ/b at 27 Mb/s With Channel Selection Based on Adaptive FBB and Digitally Programmable Pulse Shaping," *IEEE Journal of Solid-State Circuits*, vol. 52, no. 4, pp. 1163-1177, Apr. 2017.

[8] L. Smaïni, C. Tinella, D. Hélal, C. Stoecklin, L. Chabert, C. Devaucelle, R. Cattenoz, N. Rinaldi, and D. Belot, "Single-Chip CMOS Pulse Generator for UWB Systems," *IEEE Journal of Solid-State Circuits*, vol. 41, no. 7, pp. 1551-1561, Jul. 2006.

[9] L. Xia, K. Shao, H. Chen, Y. Huang, Z. Hong, and P. Y. Chiang, "5-nJ/b 3–5-GHz IR-UWB System With Spectrum Tunable Transmitter and Merged-Correlator Noncoherent Receiver," *IEEE Transactions on Microwave Theory and Techniques*, vol. 59, no. 4, pp. 1147-1156, Apr. 2011.

[10] S. Gambini, J. Crossley, E. Alon, and J. M. Rabaey, "A Fully Integrated, 290 pJ/bit UWB Dual-Mode Transceiver for cm-Range Wireless Interconnects," *IEEE Journal of Solid-State Circuits*, vol. 47, no. 3, pp. 586-598, Mar. 2012.

[11] L. B. Leene, S. Luan, and T. G. Constandinou, "A 890fJ/bit UWB transmitter for SOC integration in high bit-rate transcutaneous bio-implants," in *Proceeding of 2013 IEEE International Symposium on Circuits and Systems*, pp. 2271-2274, May 2013.

[12] O. Fourquin, S. Bourdel, J. Gaubert, R. Vauché, N. Dehaese, A. Chami, J.-Y. Dauvignac, G. Kossiavas, N. Fortino, and P. Brachat, "Chip On Board 3–10-GHz Impulse Radio Ultra Wideband Transmitter With Optimized Die to Antenna Wire Bond Transition," *IEEE Transactions on Components, Packaging and Manufacturing Technology*, vol. 3, no. 5, pp. 749-758, May 2013.

[13] K. K. Lee, and T. S. Lande, "A 2.8–7.5 pJ/Pulse Highly-Flexible Impulse-Radio Ultra-Wideband Pulse-Generator," *Progress In Electromagnetics Research C*, Vol. 55, 139-147, 2014.

[14] K. Ture, A. Devos, F. Maloberti, and C. Dehollain, "Area and Power Efficient Ultra-Wideband Transmitter Based on Active Inductor," *IEEE Transactions on Circuits and Systems II: Express Briefs*, vol. 65, no. 10, pp. 1325-1329, Oct. 2018.

[15] Z. Zhang, Y. Li, G. Wang, and Y. Lian, "The Design of an Energy-Efficient IR-UWB Transmitter With Wide-Output Swing and Sub-Microwatt Leakage Current," *IEEE Transactions on Circuits and Systems II: Express Briefs*, vol. 65, no. 10, pp. 1485-1489, Oct. 2018.

[16] D. D. Wentzloff, and A. P. Chandrakasan, "A 47pJ/pulse 3.1-to-5GHz All-Digital UWB Transmitter in 90nm CMOS," in *Proceeding of 2007 IEEE International Solid-State Circuits Conference Digest of Technical Papers*, pp. 118-119, Feb. 2007.

[17] Y. Park, and D. D. Wentzloff, "An All-Digital 12 pJ/Pulse IR-UWB Transmitter Synthesized From a Standard Cell Library," *IEEE Journal of Solid-State Circuits*, vol. 46, no. 5, pp. 1485-1489, May 2011.

[18] H. Hedayati, and K. Entesari, "A 90-nm CMOS UWB Impulse Radio Transmitter With 30-dB In-Band Notch at IEEE 802.11a System," *IEEE Transactions on Microwave Theory and Techniques*, vol. 61, no. 12, pp. 4220-4232, Dec. 2013.

[19] J. R. Long, "Monolithic Transformers for Silicon RF IC Design," *IEEE Journal of Solid-State Circuits*, vol. 35, no. 9, pp. 1368-1382, Sep. 2000.

[20] J.-W. Lee, L. F. Eastman, and K. J. Webb, "A Gallium-Nitride Push-Pull Microwave Power Amplifier," *IEEE Transactions on Microwave Theory and Techniques*, vol. 51, no. 11, pp. 2243-2249, Nov. 2003.

[21] Y. Zheng, Y. Tong, C. W. Ang, Y.-P. Xu, W. G. Yeoh, F. Lin, and R. Singh, "A CMOS Carrierless UWB Transceiver for WPAN Applications," in *Proceeding of 2006 IEEE International Solid-State Circuits Conference Digest of Technical Papers*, pp. 378-387, Feb. 2006.

[22] P. Gunturi, N. W. Emanetoglu, and D. E. Kotecki, "A 250-Mb/s Data Rate IR-UWB Transmitter Using Current-Reused Technique," *IEEE Transactions on Microwave Theory and Techniques*, vol. 65, no. 11, pp. 2243-2249, Nov. 2017.

Nontapat Channarong received his Bachelor degree in Electronics Engineering from King Mongkut's Institute of Technology Ladkrabang (KMITL), Bangkok, Thailand, in 2015. He is currently pursuing his Master degree at the same university. His research interests include CMOS IC design, particularly at high frequencies, and Impulse Radio technology.

Kritsapon Leelavattananon received his Bachelor's degree in Electrical Engineering from Chiang Mai University, Chiang Mai, Thailand, and his PhD degree in Electronics Engineering from Imperial College London, London, UK. He is currently a lecturer at the Department of Electronics Engineering, King Mongkut's Institute of Technology Ladkrabang (KMITL), Bangkok, Thailand. His research interests include Analogue, Mixed Signal and RF integrated circuits design.